

# Associative ionization in a dilute ultracold ${}^7\text{Li}$ gas probed with a hybrid trap

N. Joshi,<sup>1,†,\*</sup> Vaibhav Mahendrakar,<sup>1,†</sup> M. Niranjana,<sup>1,2,†</sup> Raghuveer Singh Yadav,<sup>1</sup>

E Krishnakumar,<sup>1</sup> A. Pandey<sup>3</sup>, R Vexiau<sup>3</sup>, O. Dulieu<sup>3</sup>, S. A. Rangwala<sup>1,\*</sup>

<sup>1</sup>Raman Research Institute, C. V. Raman Avenue, Sadashivanagar, Bangalore 560080, India

<sup>2</sup>Laboratoire Charles Fabry, Institut d'Optique, CNRS, Université Paris-Saclay, 91127 Palaiseau, France

<sup>3</sup>Laboratoire Aimé Cotton, CNRS, Université Paris-Saclay, Orsay, 91400, France

(Dated: November 5, 2024)

The formation of  $\text{Li}_2^+$  and subsequently  $\text{Li}^+$  ions, during the excitation of  ${}^7\text{Li}$  atoms to the  $3S_{1/2}$  state in a  ${}^7\text{Li}$  magneto optical trap (MOT), is probed in an ion-atom hybrid trap. Associative ionization occurs during the collision of  $\text{Li}(2P_{3/2})$  and  $\text{Li}(3S_{1/2})$  ultracold atoms, creating  $\text{Li}_2^+$  ions. Photodissociation of  $\text{Li}_2^+$  by the MOT lasers is an active channel for the conversion of  $\text{Li}_2^+$  to  $\text{Li}^+$ . A fraction of the  $\text{Li}_2^+$  ions is long lived even in the presence of MOT light. Additionally, rapid formation of  $\text{Li}^+$  from  $\text{Li}_2^+$  in the absence of MOT light is observed. Resonant excitation of ultracold atoms, resulting in intricate molecular dynamics, reveals important processes in ultracold dilute gases.

Experiments with hybrid ion-atom traps, which combine laser-cooled ions with ultracold neutral atoms have opened up new possibilities for studying complex interactions and processes [1–15]. In such systems the products of ion-atom collisions can be trapped, leading to unprecedented details of interaction outcomes [16–24]. One can measure collision rates and branching ratios of competing channels [2, 25–35] leading to the discovery of processes previously undetected in beam experiments.

In this article we use a hybrid trap as a tool to probe the formation of  $\text{Li}_2^+$  and subsequently  $\text{Li}^+$  ions when a low intensity and narrow linewidth laser at 813 nm, resonant with the  $2P_{3/2} \rightarrow 3S_{1/2}$  transition in  ${}^7\text{Li}$  is incident on a magneto optical trap (MOT) of  ${}^7\text{Li}$ . These processes have not been reported in former ultracold  ${}^7\text{Li}$  atom experiments, and in beam experiments that employed the  $2P \rightarrow 3S$  excitation [36–39], as an intermediate step, for producing lithium Rydberg atoms. Below, we report a series of measurements, and employ electronic structure calculations on  $\text{Li}_2$  and  $\text{Li}_2^+$  as well as computation of  $\text{Li}_2^+$  photodissociation rates for understanding our experimental observations.

Our hybrid trap experiment (Fig. 1(a)), consists of a  ${}^7\text{Li}$  MOT created at the center of a linear Paul trap with 4 linear, and 2 dc endcap electrodes. The MOT typically contains  $1.7 \times 10^6$  atoms, with a density of  $5.6 \times 10^{14}$  atoms/ $\text{m}^3$  at a temperature of 500  $\mu\text{K}$ . The values of the red detuning of the cooling laser ( $\Delta_c$ ) from the  $2S_{1/2}(F=2) \rightarrow 2P_{3/2}(F=3)$  transition, and of the repumping laser ( $\Delta_r$ ) from the  $2S_{1/2}(F=1) \rightarrow 2P_{3/2}(F=2)$  transition (Fig 1(b)), are  $\Delta_c \approx -38$  MHz, and  $\Delta_r \approx -22$  MHz. The total cooling and repumping intensities are  $\approx 77$  mW/ $\text{cm}^2$  and  $\approx 25$  mW/ $\text{cm}^2$  respectively and the magnetic field gradient is 13.6 Gauss/cm. More details on the MOT operation are provided in the Supplemental material (SM). The Paul trap is operated

with an angular frequency and amplitude of rf ( $\Omega_{rf}$ ,  $V_{rf}$ ) applied to one diagonal pair of electrodes while the other pair is grounded [40, 41]. The end cap electrodes are at constant potential  $V_{ec}$ . The ions, once created are trapped in the ion trap and extracted onto a microchannel plate (MCP) by switching off the rf voltage at zero phase, while simultaneously applying a brief, negative high voltage (HV) pulse to the grid electrode (see Fig. 1 (a)). Ions hitting the MCP build a time of flight (ToF) mass spectrum and can be counted (Fig. 2).

The experiment is conducted as follows. The  ${}^7\text{Li}$  MOT is loaded under standard conditions while the ion trap is kept on with operating parameters  $V_{rf} = 70$  V,  $\Omega_{rf}/2\pi = 1$  MHz,  $V_{ec} = 4$  V (Configuration A, Table II in SM). When an 813 nm narrow linewidth laser driving the  $2P_{3/2} \rightarrow 3S_{1/2}$  ( $F=1$  or  $F=2$ ) transition of

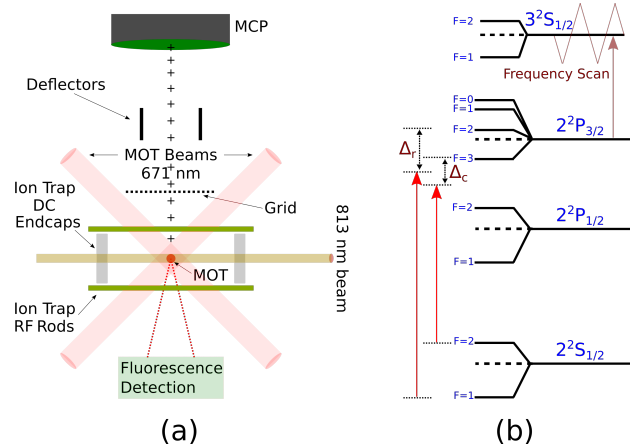


FIG. 1. (a) Schematic representation of the experimental setup. The MOT is positioned at the ion trap center. (b) Energy level diagram of  ${}^7\text{Li}$  for the MOT operation and for the excitation of the MOT atoms to the  $3S_{1/2}$  state. The  $3S_{1/2} \rightarrow 2P_{3/2}$  fluorescence is monitored by scanning the 813 nm laser across the  $2P_{3/2} \rightarrow 3S_{1/2}$  transition frequency (see SM for details). See SM for details of the fluorescence detection optical setup.

\* Email: njoshi@rri.res.in; sarangwala@rri.res.in

† Contributed equally

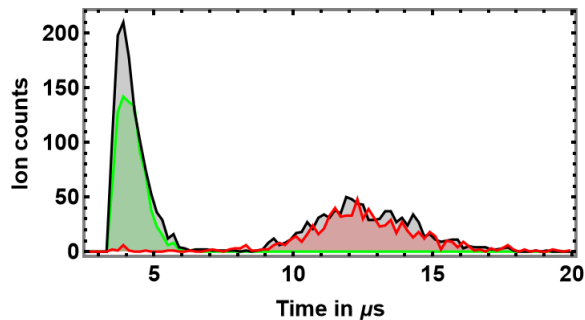


FIG. 2. ToF spectrum, recorded in configuration A (see SM), of the ions created by the 813 nm laser (black curve) and the UV LED (green curve). The red curve shows a loss of the 813 nm generated ions, which appear at the same ToF as the UV LED generated ions, in the presence of a parametric frequency  $f_p(\text{Li}^+) = 149$  kHz (Table I).

$^7\text{Li}$  MOT atoms is turned on (see Fig. 1(b) and SM), and the above extraction sequence is followed, a mass spectrum exhibiting two peaks is observed (Fig. 2 black curve). When only the MOT is operational, no ions are produced and detected upon extraction. The narrow peak at  $\approx 4\mu\text{s}$  is assigned to the  $\text{Li}^+$  signal, as it coincides with the peak (green curve in Fig. 2) recorded when a sole UV LED (M340L4 Thorlabs) is employed to directly photoionize the  $\text{Li}(2P_{3/2})$  atoms in the MOT. The broad distribution around  $12\mu\text{s}$  could be induced by any ion with a mass larger than that of the  $\text{Li}^+$  monomer, including  $\text{Li}_m^+$  ions with  $m > 1$ . Due to the pulsed grid extraction, the ToF of the detected ions does not scale as the square root of ion masses. We, therefore, use the parametric excitation (PE) technique [42, 43] to characterize the broad distribution. A small perturbation with a frequency  $f_p$  is applied to the trapped ions. The energy transfer to the ion is maximum when  $f_p$  is twice the secular frequency  $f_s$  of the trapped ions. A PE resonance is detected when the ions of a particular charge-to-mass ratio ( $Q/M$ ) are rapidly ejected from the trap, leaving ions with different ( $Q/M$ )' unaffected. By tuning  $f_p$ , the trapped ions for various ( $Q/M$ ) can be selectively emptied (see SM). We first load the trap from MOT atoms by pulsing the UV LED for a short time interval and determine the PE resonance,  $f_p(\text{Li}^+)$ , for  $\text{Li}^+$  by tuning  $f_p$  in the configuration A (see Table II in SM). To determine PE resonance frequency for  $\text{Li}_m^+$  ions created when applying the 813 nm laser, we eliminate  $\text{Li}^+$  by tuning the extraction pulse on the grid electrode such that the trapped  $\text{Li}^+$  ions do not reach the detector while  $\text{Li}_m^+$  ions do (configuration B, Table II in SM). Then  $f_p$  is tuned to locate the PE resonance,  $f_p(\text{Li}_m^+)$ , for  $\text{Li}_m^+$ . The ratio  $f_p(\text{Li}^+)/f_p(\text{Li}_m^+)$  is determined for different values of  $V_{ec}$  and converges to 2 when  $V_{ec} \rightarrow 0$  (see Table I and [44]). This establishes that the broad distribution peaked at  $12\mu\text{s}$  in Fig. 2 contains  $\text{Li}_2^+$  ions.

We investigate the formation mechanism of the  $\text{Li}^+$  and  $\text{Li}_2^+$  ions which appears to be a complex process induced

by the excited Li atoms. The ionization energy of the  $2P_{3/2}$  and  $3S_{1/2}$  levels does not allow the creation of  $\text{Li}^+$  by single photon ionization of lithium atoms from these levels by the 670 nm or 813 nm lasers. In addition, multiphoton ionization is unlikely as there is no resonant intermediate state to enhance ionization [45, 46]. This raises the issue of the origin of the  $\text{Li}^+$  ions. First, in configuration A (see SM), we observe that in the presence of a parametric drive at 149 kHz (Table I) there is a loss of the 813 nm generated ions that have the same ToF as the UV LED generated  $\text{Li}^+$  ions (red curve in Fig. 2), reconfirming that this fraction of the ions is indeed  $\text{Li}^+$ . We further test whether the 813 nm excitation generates only  $\text{Li}_2^+$  to begin with. In configuration A while shining the 813 nm laser, the application of  $f_p(\text{Li}_m^+) = 65$  kHz eliminates both the  $\text{Li}^+$  and  $\text{Li}_2^+$  peaks in the ToF spectrum of Fig. 2, except for rare counts at the ToF of  $\text{Li}^+$ . In contrast, the  $\text{Li}^+$  ions created with the UV LED are unaffected by the 65 kHz excitation, as determined in a separate experiment. This strongly indicates that the  $\text{Li}^+$  ions are created from  $\text{Li}_2^+$  and the ions in the broad peak are  $\text{Li}_2^+$  exclusively. For this experiment, the PE of the  $\text{Li}_2^+$  ions has to be rapid so that the  $\text{Li}_2^+$  ions are ejected from the trap before a sizable fraction of  $\text{Li}^+$  forms. This required the PE amplitude of  $\text{Li}_2^+$  to be increased by  $\approx 9.3$  times the typical value (Table I).

To identify the process leading to  $\text{Li}_2^+$  production, we calculate the potential energy curves (PECs) for  $\text{Li}_2$  and  $\text{Li}_2^+$  (Fig. 3), using the same methodology as reported earlier [47, 48]. A colliding pair of  $2P_{3/2}$  and  $3S_{1/2}$  atoms have enough energy to reach the  $\text{Li}_2$  ionization threshold undergoing associative ionization (AI) [49–59], which occurs due to autoionization of the two interacting excited atoms scattering along several PECs which asymptotically correlate to the  $2P_{3/2} + 3S_{1/2}$  dissociation limit. A fraction of these colliding pairs generates  $\text{Li}_2^+$ , and the rest radiatively decays back to ground atomic states. By tuning the 813 nm laser over a range of frequencies  $> 100$  GHz across the  $2P_{3/2} \rightarrow 3S_{1/2}$  resonance, the  $\text{Li}_2^+$  signal manifests only when the sum of the photon energies of the 670 nm and 813 nm laser equals the energy difference between the  $2S_{1/2}$  and  $3S_{1/2}$  atomic levels. This weighs against other processes that involve, as an intermediate step, the photoassociation (PA) of neutral  $\text{Li}_2$  in a

TABLE I. Comparison of the most prominent resonant frequency for  $\text{Li}^+$  and  $\text{Li}_m^+$  measured by varying the frequency of the parametric drive ( $f_p$ ), in steps of 1 kHz and recording the number of ions reaching the MCP at each frequency value. The peak-to-peak parametric drive amplitude, in units of milli volts ( $mV_{pp}$ ), is kept to be 180  $mV_{pp}$  and 67.5  $mV_{pp}$  respectively, for the  $\text{Li}^+$  and the  $\text{Li}_m^+$ .

$V_{ec}$ (V)	$f_p(\text{Li}^+)$ (kHz)	$f_p(\text{Li}_m^+)$ (kHz)	$f_p(\text{Li}^+)/f_p(\text{Li}_m^+)$
4	$149 \pm 0.5$	$65 \pm 0.5$	$2.29 \pm 0.03$
2	$155 \pm 0.5$	$72 \pm 0.5$	$2.15 \pm 0.02$
1	$158 \pm 0.5$	$76 \pm 0.5$	$2.08 \pm 0.02$

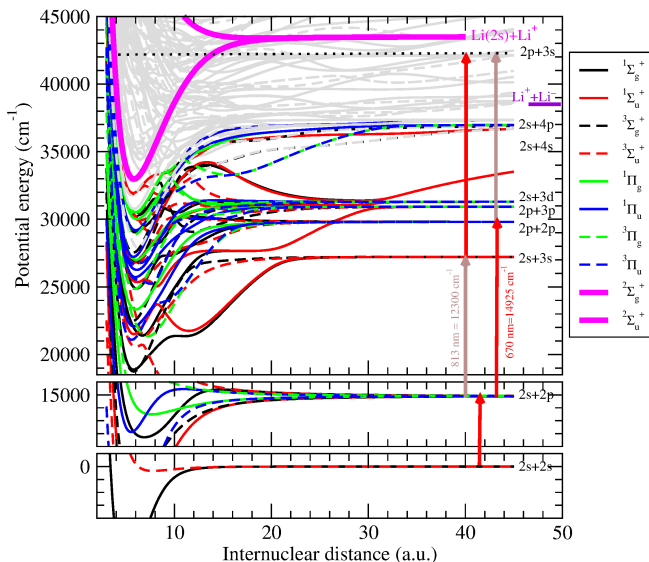


FIG. 3. PECs of  $\text{Li}_2$  ground and excited electronic states up to the energy range of the lowest  $\text{Li}_2^+$  PECs (thick full magenta lines), computed according to [47, 48]. The energy of the  $\text{Li}^+ + \text{Li}^-$  is indicated for completeness. The grey curves illustrate the complexity of the PECs of highly excited states, which are irrelevant at short distances when they enter the ionization continuum. The arrows picture the possible excitation pathways of the Li atoms.

specific bound rovibrational level which can either be photoionized (PI) directly (PA-PI [60]) at short range or can be further excited to an autoionizing state, commonly referred to as photoassociative ionization (PAI) [61]. From Fig. 3, it is impossible to identify the molecular states responsible for AI, as the relevant energy zone close to the  $2P_{3/2} + 3S_{1/2}$  dissociation limit corresponds to highly-excited states with adiabatic PECs which have a poor accuracy at short distances, as they cross the ionization threshold (grey curves in Fig. 3). Based on the calculated PECs, we infer that the  $\text{Li}_2^+$  ions are created in the  $X^2\Sigma_g^+$  ground electronic state with a vibrational level not higher than  $v_g = 50$ , with a binding energy of about  $1000 \text{ cm}^{-1}$  or more. We measured the total number of created  $\text{Li}_2^+$  and  $\text{Li}^+$  ions for constant MOT density, which is linear with the intensity of the 813 nm laser, indicating that a single photon is involved (see SM and [62]). For a constant 813 nm laser intensity, the number of detected ions varies quadratically with the MOT density, which is the signature of a two-atom process (see SM and [63]).

As invoked above, the  $\text{Li}^+$  yield must originate from the  $\text{Li}_2^+$  ions. Two options are plausible: (i) photodissociation of  $\text{Li}_2^+$  by the MOT lasers [18] or by the 813 nm laser; (ii) charge exchange with neutral Li atoms [64]. Another possibility of creating  $\text{Li}^+$  which does not involve the formation of  $\text{Li}_2^+$  in the  $X^2\Sigma_g^+$  state, is the autoionization of colliding  $3S_{1/2} + 3S_{1/2}$  atoms along the lowest  $A^2\Sigma_u^+$  dissociative  $\text{Li}_2^+$  PEC. This was the major pathway for the formation of atomic ions in a previous study employ-

ing a similar scheme for exciting Rubidium MOT atoms and was referred to as photoassociative dissociative ionization (PADI) [62].

We study the ion population dynamics with the ion trap and HV extraction pulse set up in configuration A (see SM), which is suitable for trapping and detecting both  $\text{Li}^+$  and  $\text{Li}_2^+$ . The MOT atoms are irradiated by a 10 ms pulse of the 813 nm laser with  $5 \text{ mW/cm}^2$  intensity. The created ions are held in the ion trap, in the presence of MOT atoms, for varying holding times of duration 10 ms and longer, and extracted toward the MCP (Fig. 4). In panels (a)-(d), we see that the population of  $\text{Li}^+$  increases with increasing holding times, while the  $\text{Li}_2^+$  population decreases. Panel (e) shows that after a fast decrease (increase) of the  $\text{Li}_2^+$  ( $\text{Li}^+$ ) signal, the mean number of each ion species stabilizes over long holding times (see SM for the counting methodology). This experiment confirms that as time progresses, the  $\text{Li}_2^+$  ions are converted into  $\text{Li}^+$  ions. The measured small number of  $\text{Li}^+$  for the 10 ms holding time measurement (Fig. 4a) reflects the negligible population of the  $3S_{1/2} + 3S_{1/2}$  scattering channel, which would directly produce  $\text{Li}^+$  via PADI.

We next investigate the photodissociation (PD) of  $\text{Li}_2^+$  by the MOT lasers. In Fig. 5(a) we display the computed PD cross section and rate [18, 65] at 670 nm of the  $\text{Li}_2^+$  ground electronic state ( $X^2\Sigma_g^+$ ) vibrational levels

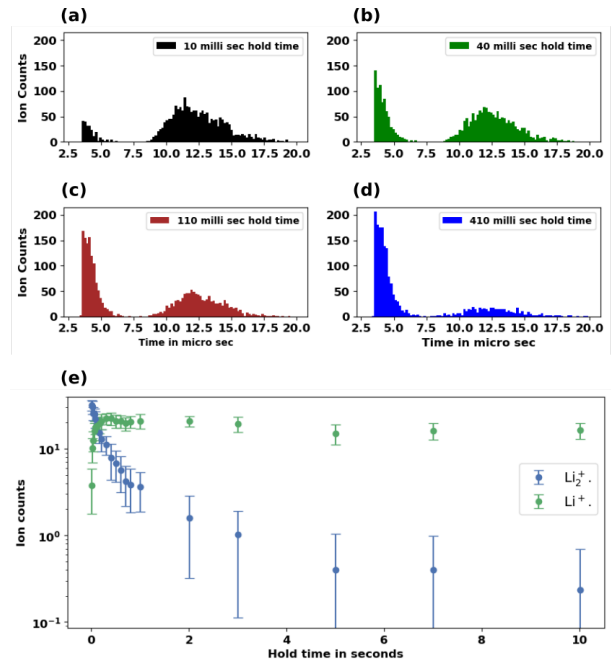


FIG. 4. (a-d) ToF spectra of the ions generated by the 813 nm laser pulse, for increasing holding times in the presence of the MOT. Hold time is measured with respect to the rising edge of the 813 nm pulse. In the ToF spectra, we identify the signal below and above  $7 \mu\text{s}$  as  $\text{Li}^+$  and  $\text{Li}_2^+$  respectively (see SM). For each holding time, 60 measurements are performed and used to construct the histograms. (e) Variation of the mean number of  $\text{Li}^+$  and  $\text{Li}_2^+$  ions per shot with the holding time. The error bars represent one standard deviation.

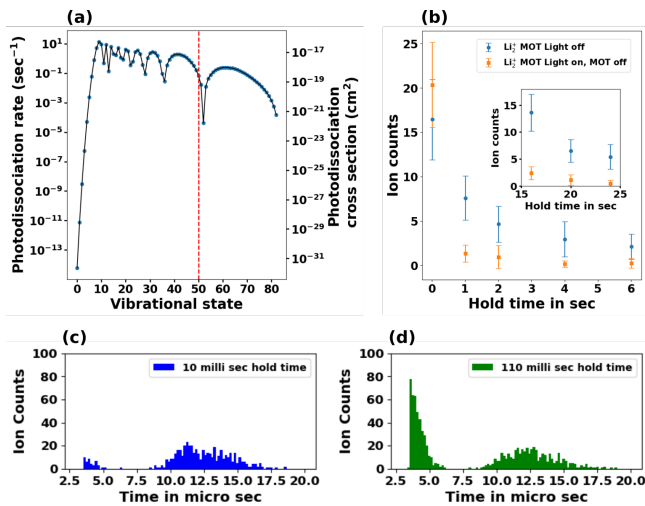


FIG. 5. (a) Calculated  $\text{Li}_2^+$  PD cross section and non-thermalized rate at 670 nm for the vibrational levels of the  $^2\Sigma_g^+$  ground state toward the dissociation continuum of the lowest  $^2\Sigma_u^+$  state. The red dashed line marks the  $v_g = 50$  vibrational level, which is the highest level that can be populated when entering by the  $2P_{3/2} + 3S_{1/2}$  scattering channel. (b) Lifetime measurements of  $\text{Li}_2^+$  made in configuration C (see Table II in SM) in the presence and absence of the MOT laser. The inset shows the existence of long lived  $\text{Li}_2^+$  ions in the presence of MOT light. Panels (c) and (d) show the change in ToF spectra indicating conversion of  $\text{Li}_2^+$  to  $\text{Li}^+$  even in the absence of MOT light. The MOT level was not ensured to be the same in (c) and (d) as we just wanted to depict change in the ToF.

toward the dissociation continuum of the  $A^2\Sigma_u^+$  state, using the PECs of Fig. 3. We see that the few lower vibrational levels cannot be photodissociated by the 670 nm light due to a large binding energy. If populated, these ions will have a long lifetime in the trap, unlike the  $\text{Rb}_2^+$  case where all levels were affected by the MOT light [18]. To probe the photodissociation of  $\text{Li}_2^+$ , we perform measurements similar to those of Fig. 4, operating the ion trap in configuration C (Table II in SM), which traps only  $\text{Li}_2^+$ . The MOT is loaded for 20 s, and the 813 nm laser with 5 mW/cm<sup>2</sup> intensity is switched on for 10 ms just before switching off the repumper and emptying the MOT. In 10 ms, more than 70% of the MOT atoms leave the volume of the overlapping MOT beams as determined experimentally using the release and recapture method [66]. The ions created by the 813 nm laser are held in the ion trap for various duration either in the presence or in the absence of the MOT cooling light, and are extracted toward the MCP. The results clearly indicate that the molecular ions have a much shorter lifetime in the presence of MOT light, which then contributes to the loss of  $\text{Li}_2^+$  (Fig. 5(b)). We neglect the PD of  $\text{Li}_2^+$  due to the 813 nm laser as its intensity is very small compared to the MOT lasers and also it is pulsed only for a short time. Further, a laser with a wavelength  $\leq 444$  nm can photodissociate even the lowest vibrational level of  $\text{Li}_2^+$  which, due to larger binding energy, is immune from PD

by the 670 nm light. We indeed observe a lower lifetime if the  $\text{Li}_2^+$  ions are exposed to both the 670 nm and a 420 nm laser.

We further investigated the presence of long lived molecular ions in the presence of the MOT light. The pulse width of the 813 nm laser was increased to 500 ms to produce a large number of ions so that, statistically, a sizable fraction of the ions may be generated in low vibrational levels and thus with a low photodissociation rate. The results of the measurements are shown in the inset of Fig. 5(b). We present data only at large holding times because the counting of ions at small holding times is not possible due to MCP saturation.

From Fig. 5(b), we also observe a rapid decrease in the number of  $\text{Li}_2^+$  in going from 10 ms to 1 s holding time even in the absence of MOT light. Since this loss is not due to the trap lifetime, we probe the short timescale dynamics in the absence of MOT light. The measurements, similar to the ones in Fig. 5(b), were made in configuration A which traps both  $\text{Li}^+$  and  $\text{Li}_2^+$ . We present two measurements, shown in Fig. 5(c) and 5(d): they indicate a change in the ToF histograms at different hold times and signals the presence of another process, which leads to the initial, non-optical rapid conversion of  $\text{Li}_2^+$  to  $\text{Li}^+$ . The cause of this rapid conversion is yet to be explored as it cannot be further probed in the present experiment. We theoretically evaluated the rates of charge exchange of  $\text{Li}_2^+$  with background Li atoms by considering the Langevin collision model [67, 68]. However, the collision rates are small with both the background as well as MOT atoms to explain the fast conversion of  $\text{Li}_2^+$  to  $\text{Li}^+$  in Fig. 5(b) and Fig. 4(e). We have also observed the formation of  $\text{Li}_2^+$  ions in driving the  $2P \rightarrow 3S$  transition in a  $^6\text{Li}$  MOT by the 813 nm laser. Signatures of the formation of  $\text{Li}_2^+$  were reported earlier in a  $^6\text{Li}$  MOT illuminated with a femtosecond laser having a 750 nm–820 nm spectral range [69].

In summary, we have shown that the simple process of resonant excitation from the first excited state of Li atoms in a dilute ultracold gas leads to rich dynamics with a large probability of formation of molecular and atomic ions. This has important implications for cold dilute and degenerate gas experiments, where photoexcitation is used [70–72], and for Rydberg atom experiments in general [36–39]. How prevalent such processes are for other commonly studied species in cold dilute gases needs to be investigated. Additionally, our results demonstrate a convenient method of loading homonuclear molecular ions in an ion trap for further cold chemistry studies. A similar methodology can be explored in the future for loading heteronuclear molecular ions as well [52, 57].

## ACKNOWLEDGMENTS

We acknowledge support from the Ministry of Electronics and Information Technology (MeitY), Govern-

ment of India, under Centre for Excellence in Quantum Technologies grant with Ref. No. 4(7)/2020-ITEA. The Workshop and Meena M S at RRI, and Jankee Upadhaya and Sudhir Kumar from RRCAT Indore for electronics support. EK acknowledges the DAE Raja Ramanna Fellowship.

## SUPPLEMENTAL MATERIAL

### I. OPTICAL DETECTION SETUP FOR THE FLUORESCENCE DETECTION OF ATOMS.

Fig 6(a) shows the optical detection setup for detecting the  $2P \rightarrow 2S$  fluorescence for MOT characterization. Fig 6(b) shows the optical detection setup for detecting the  $2P \rightarrow 3S$  excitation via the  $3S \rightarrow 2P$  fluorescence.

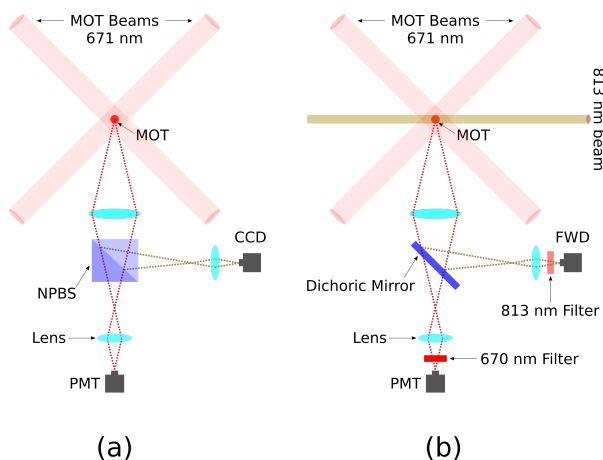


FIG. 6. (a) The characterization of the MOT (size, density, and temperature), as mentioned in the main text, was made using the  $2P \rightarrow 2S$  fluorescence collected via a 2-inch lens, mounted outside the vacuum chamber. Using a non-polarizing beam splitter (NPBS) a part of the fluorescence is sent to a CCD camera and the other part to a photomultiplier tube (PMT). (b) The detection of the  $2P \rightarrow 3S$  transition is made using the  $3S \rightarrow 2P$  fluorescence. The NPBS is replaced by a dichroic mirror which separates the  $3S$  emission line fluorescence from the MOT fluorescence and sends it to the femtowatt detector (FWD). The MOT fluorescence is detected by the PMT. The FWD and PMT additionally have 10 nm bandpass filters placed in front of them.

### II. $3S$ TO $2P$ FLUORESCENCE

Fig. 7 shows a typical fluorescence spectrum obtained by scanning the 813 nm laser across the  $2P_{3/2} \rightarrow 3S_{1/2}$  resonance. The fluorescence of atoms decaying from the  $3S_{1/2}$  state to the intermediate  $2P_{3/2}$  and  $2P_{1/2}$  states is collected on a femtowatt detector (FWD) as shown in Fig. 1(b). The peaks labeled "1c" and "2c" arise from atoms decaying from the  $3S_{1/2}(F=1)$  and  $3S_{1/2}(F=2)$

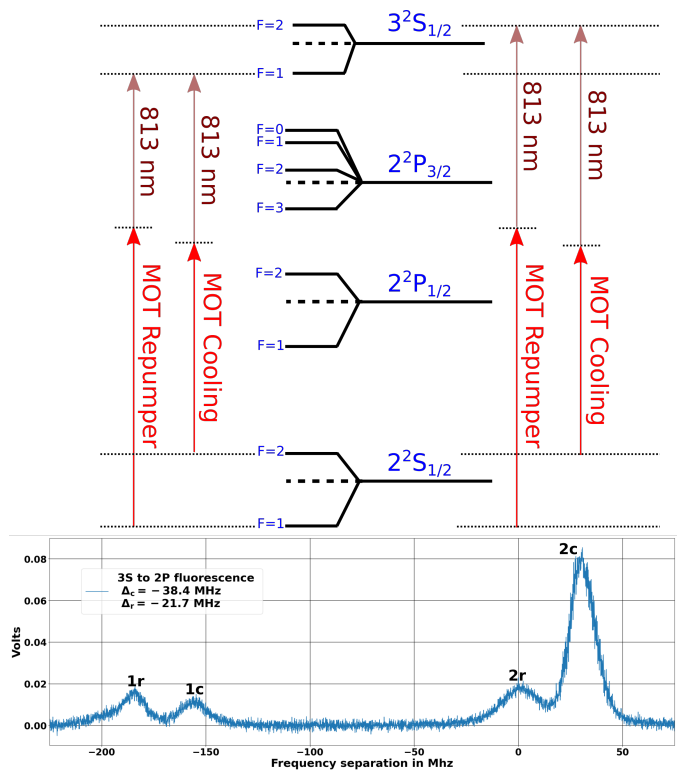


FIG. 7.  $3S$  to  $2P$  fluorescence peaks are shown aligned with their respective excitation by the MOT lasers and the 813 nm laser, as the 813 nm laser is scanned across the  $2P_{3/2} \rightarrow 3S_{1/2}$  resonance.  $\Delta_c$  and  $\Delta_r$  are the detunings of the MOT cooling and repumper lasers from the  $2S_{1/2}(F=2) \rightarrow 2P_{3/2}(F=3)$  and  $2S_{1/2}(F=1) \rightarrow 2P_{3/2}(F=2)$  transitions.

states respectively, when they were excited to these states by absorbing 2 photons, one from the MOT cooling laser and the other from the 813 nm laser. Likewise, the fluorescence peaks labeled "1r" and "2r" are due to atoms decaying from the  $3S_{1/2}(F=1)$  and  $3S_{1/2}(F=2)$  states respectively when they were excited to these states by absorbing 2 photons, one from the MOT repumper laser and the other from the 813 nm laser. The peak heights are different due to differences in the 2 photon transition strengths as different hyperfine states of the  $2P_{3/2}$  manifold are involved in the transition. The 2c-1c and 2r-1r peak separations are in agreement with the  ${}^7\text{Li}$  hyperfine splitting of the  $3S_{1/2}$  state [73]. For all the measurements in the main text, the 813 nm laser was locked on the 2c peak. But we observe molecular ions at other peak values as well.

### III. DETECTION OF TRAPPED IONS

For detecting trapped ions, the RF on the cylindrical electrodes is switched off at zero phase, and simultaneously a negative high voltage (HV) pulse is applied to the grid electrode to pull the ions towards the MCP (Fig. 1(a) in the main text). Pulsed HV is required to prevent

the ions that have crossed the grid from being pulled back towards the grid. Therefore the duration ( $t_{HV}$ ) and height ( $V_{HV}$ ) of the pulse need to be adjusted accordingly. Additionally, the pulse duration and height can be adjusted so that ions of a certain charge to mass ( $Q/M$ ) ratio reach the MCP but others do not, as the grid voltage pulls them back. We have used this for differentiating between the ions generated by the LED and the 813 nm laser in Section IV below and also in probing ion resonances using parametric excitation as described in Section V below.

#### IV. CONFIGURATIONS DISTINGUISHING THE LED AND 813 NM GENERATED IONS

Configuration A, in Table II below, is the typical ion trapping and extraction configuration in our experimental setup. In this configuration, the ToF spectrum of the  $\text{Li}^+$  ions generated by the UV LED and that of the 813 nm laser generated ions is respectively the green and black curves in Fig. 2 in the main text. Configurations B and C (Table II) are designed to distinguish between the  $\text{Li}^+$  ions, and the  $\text{Li}_m^+$  ions which appear as a diffuse peak in the black curve in Fig. 2 in the main text.

In configuration B, the ion trap parameters are kept the same as in configuration A, but the height ( $V_{HV}$ ) and duration ( $t_{HV}$ ) of the negative HV pulse on the grid is increased so that the  $\text{Li}^+$  ions do not reach the MCP. In configuration C, the negative high voltage pulse characteristics are kept the same as in configuration A, but the ion trap parameters are adjusted to lie outside the ion trap stability region of  $\text{Li}^+$ . Configurations A and B are used in the parametric excitation measurements in Section V below.

TABLE II. A, B, and C are configurations designed to distinguish between the LED and 813 nm generated ions.  $V_{rf}$  and  $\Omega_{rf}$  is respectively the rf voltage and angular frequency applied to one pair of diagonal rf electrodes and the other pair is grounded.  $V_{ec}$  is the voltage applied to the endcaps.  $V_{HV}$  and  $t_{HV}$  is respectively the height and duration of the HV pulse on the grid electrode.

	$V_{rf}$ (V)	$\Omega_{rf}/2\pi$ (kHz)	$V_{ec}$ (V)	$V_{HV}$ (V)	$t_{HV}$ ( $\mu\text{s}$ )
A	70	1000	4	-600	1.8
B	70	1000	4	-1000	2.4
C	76	500	10	-600	1.8

#### V. ION RESONANCES USING PARAMETRIC EXCITATION.

Since the ToF's is not enough to determine the mass of  $\text{Li}_m^+$ , we use the method of parametric excitation (PE) [43] to determine the resonant frequency of  $\text{Li}_m^+$  and compare it to that of  $\text{Li}^+$ . A small amplitude ( $V_p$ ) parametric

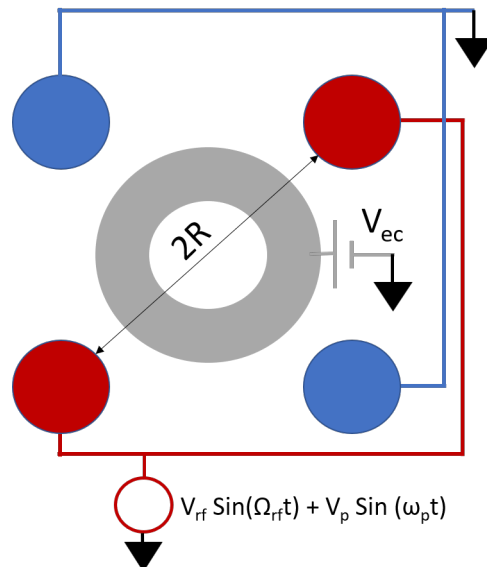


FIG. 8. Axial view of the linear Paul trap. The annular disc at the center is the endcap on which a DC voltage  $V_{ec}$  is applied. RF signal of amplitude  $V_{rf}$  and angular frequency  $\Omega_{rf}$  plus the parametric drive of amplitude  $V_p$  and angular frequency  $\omega_p$  is applied on one diagonal pair of electrodes while the other pair is grounded.

drive of a particular frequency ( $\omega_p = 2\pi f_p$ ) is mixed with  $V_{rf}$  as shown in Fig. 8. The ions, generated either via the LED or the 813 nm laser, are loaded in the ion trap for 0.5 s. Beyond this time they are held in the ion trap for another 1.5 s before getting extracted toward the MCP. This measurement is done at different parametric drive frequencies and in each case, the number of ions reaching the MCP is recorded. For comparing the resonant frequencies of the two ions, the ion trap parameters need to be the same. Configurations A and B (see Table II) have the same ion trap parameters. For the LED generated  $\text{Li}^+$  ions, we measure the resonant frequencies in configuration A, where the HV pulse characteristics are well suited for the detection of  $\text{Li}^+$ . However, for the  $\text{Li}_m^+$ , generated by the 813 nm laser, we performed measurements in configuration B where the HV pulse is adjusted so that the  $\text{Li}^+$  ions do not reach the MCP. This ensures that  $\text{Li}^+$  ions, generated via the 813 nm, do not appear as a source of background noise in the measurement of the resonant frequency of  $\text{Li}_m^+$ . For reasons explained below, we have performed measurements at  $V_{rf} = 70$  V and  $\Omega_{rf}/2\pi = 1000$  kHz but at three different values of  $V_{ec}$ . Table I, in the main text, compares the most prominent resonance for  $\text{Li}^+$  with that of  $\text{Li}_m^+$  at different endcap voltages. Fig. 9 shows the measurement achieved at  $V_{ec} = 1$  V.

We recall that in the adiabatic approximation [40–42], the ion secular frequencies in an ideal linear Paul trap, with no DC offset on the RF electrodes, are given by

$$\omega_u \approx \frac{\Omega_{rf}}{2} \sqrt{\frac{q_u^2}{2} + a_u}, \quad (1)$$

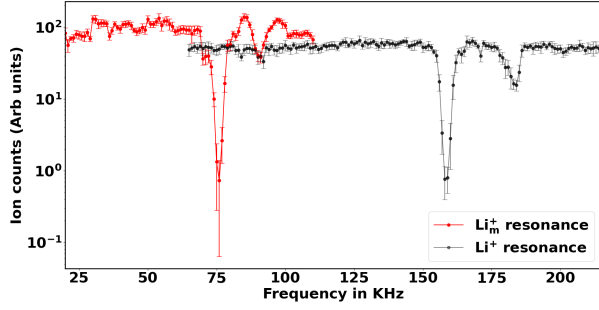


FIG. 9. Measurement of the resonances of  $\text{Li}^+$  and  $\text{Li}_m^+$  at  $V_{rf} = 70$  V and  $\Omega_{rf}/2\pi = 1000$  kHz and  $V_{ec} = 1$  V. The peak to peak parametric drive amplitude, in units of milli volts ( $mV_{pp}$ ), is  $180 mV_{pp}$  and  $67.5 mV_{pp}$  respectively, for the  $\text{Li}^+$  and  $\text{Li}_m^+$ . The amplitude of the parametric drive is kept as low as possible so that only strong resonances are visible. The frequency of the parametric drive is varied in steps of 1 kHz.

with  $u \equiv x, y, z$ , and  $(x, y)$  and  $z$  being the radial and axial directions respectively, and

$$q_x = -q_y = \frac{2QV_{rf}}{Mr_0^2\Omega_{rf}^2}, \quad (2)$$

$$q_z = 0, \quad (3)$$

$$a_x = a_y = -\frac{a_z}{2} = -\frac{4\kappa QV_{ec}}{Mz_0^2\Omega_{rf}^2}. \quad (4)$$

Here  $2r_0$  represents the surface-to-surface separation between diagonal RF electrodes (see Fig. 8),  $2z_0$  is a similar separation between the endcaps, and  $\kappa$  is a geometrical factor.  $Q$  and  $M$  are the charge and mass of the ion species. In the limit of  $V_{ec} \rightarrow 0$ , we have  $a_u \rightarrow 0$ ,  $\omega_u \rightarrow q_u \frac{\Omega_{rf}}{2\sqrt{2}}$ . The ratio of the radial secular frequency ( $\omega_{x/y}$ ) of two different ions is approximately equal to their  $(Q/M)$  ratios. This holds not only for the radial secular frequencies but also for any resonance which is not purely axial (*i.e.* which are multiples of only  $\omega_z$ ) and are of the type  $\omega_{ion} = n_1 \times \omega_{x/y} \pm n_2 \times \omega_z$ , where  $n_1$  and  $n_2$  are numbers and  $n_1 \neq 0$ . This is because  $\omega_z \rightarrow 0$  as  $V_{ec} \rightarrow 0$ . The linear Paul trap essentially behaves like a quadrupole mass spectrometer [44] in the limit of  $V_{ec} \rightarrow 0$ .

The resonances in Table I, in the main text, are radial resonances. The ratio of these resonant frequencies converges to 2.0 as the endcap voltage is lowered. This suggests that  $(Q/M)_{\text{Li}_m^+} = \frac{1}{2}(Q/M)_{\text{Li}^+}$  and that the ion generated by the 813 nm laser, which appears as a broad diffuse peak in the time of flight spectrum, is  $\text{Li}_2^+$ .

## VI. COUNTING ATOMIC AND MOLECULAR IONS IN THE HISTOGRAMS IN FIG. 4 IN THE MAIN TEXT

In Fig. 2, main text, since the diffuse ToF structure of  $\text{Li}_2^+$  has slight overlap with the ToF distribution of  $\text{Li}^+$  (green curve), we adopted the following method to count

the number of  $\text{Li}^+$  and  $\text{Li}_2^+$  ions in the histograms in Fig. 4(a) in the main text. We first build the ToF distribution of just the  $\text{Li}^+$  ions. For this purpose, for 10 ms, we load  $\text{Li}^+$  ions in the ion trap by ionizing MOT atoms in the  $2P_{3/2}$  state via the UV LED. The ions are held in the ion trap, operated in configuration A (see Table II), for another 500 ms, and are then extracted onto the MCP. 500 of such measurements are performed and the ToF distribution is recorded for each measurement. The distribution, over all these 500 measurements, is shown in Fig. 10.

For extracting the actual ToF distribution of just the molecular ions, we need to remove  $\text{Li}^+$  ions which are generated along the way and are trapped together with  $\text{Li}_2^+$ . For that purpose, we again use PE to remove  $\text{Li}^+$ . For each measurement, the MOT is loaded for 20 s. Beyond this time, the MOT light is switched off. But just before that, an amount of  $5 \text{ mW/cm}^2$  of the 813 nm light is incident on the MOT for 10 ms to create ions. The ions are held in the ion trap, for 2 s, in the presence of a parametric drive for  $\text{Li}^+$ , and are then extracted onto the MCP. These measurements are made in configuration A (see Table II). Fig. 10 shows the ToF distribution over 500 of such measurements.

We see that the ToF distributions of  $\text{Li}^+$  and  $\text{Li}_2^+$  are well separated with a very small overlap. We choose  $7 \mu\text{s}$  as the cutoff time (blue dashed vertical line in Fig. 10) for counting the number of  $\text{Li}^+$  and  $\text{Li}_2^+$  ions in Fig. 4(a) in the main text. All ions with ToF less than  $7 \mu\text{s}$  are counted as  $\text{Li}^+$  and the ones beyond this time are counted as  $\text{Li}_2^+$ .

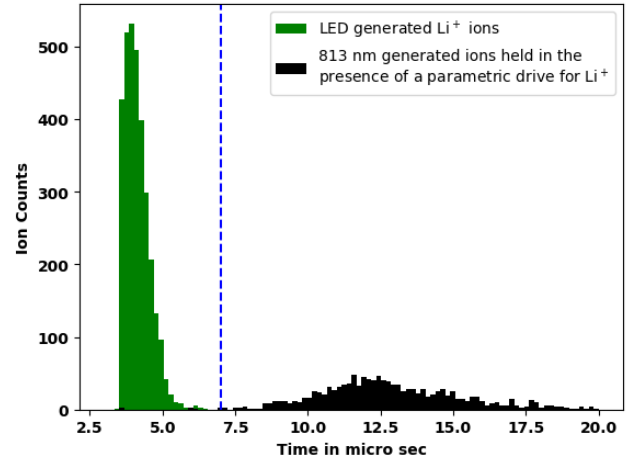


FIG. 10. ToF distribution of the  $\text{Li}^+$  and  $\text{Li}_2^+$  ions, in configuration A. The blue dashed vertical line, at  $7 \mu\text{s}$ , is the cutoff ToF. Ions before and beyond this ToF are counted as  $\text{Li}^+$  and  $\text{Li}_2^+$  respectively.

## VII. ASSOCIATIVE IONIZATION RATE

For measuring the rate of associative ionization (AI), the 813 nm laser is continuously illuminating the  ${}^7\text{Li}$  MOT atoms. Further, the ion trap electrodes are configured to continuously extract the produced ions onto the MCP. For determining the rate at which the ions are hitting the MCP the oscilloscope continuously records a total of 100 frames, each of 10 ms duration containing electronic pulses corresponding to ions hitting the MCP. For recording the variation of the AI rate with the MOT density, the intensity of the 813 nm laser is kept to  $\approx 1 \text{ mW/cm}^2$ . For measuring the variation of the rate with intensity the MOT is maintained at a density of  $\approx 10^{15} \text{ atoms/m}^3$ . The red data with error bars in Fig. 11 shows the variation of the AI rate with the 813 nm intensity and is fitted to a linear function. The blue data with error bars in Fig. 11 shows the variation of the AI rate with the MOT density and is fitted to a quadratic function.

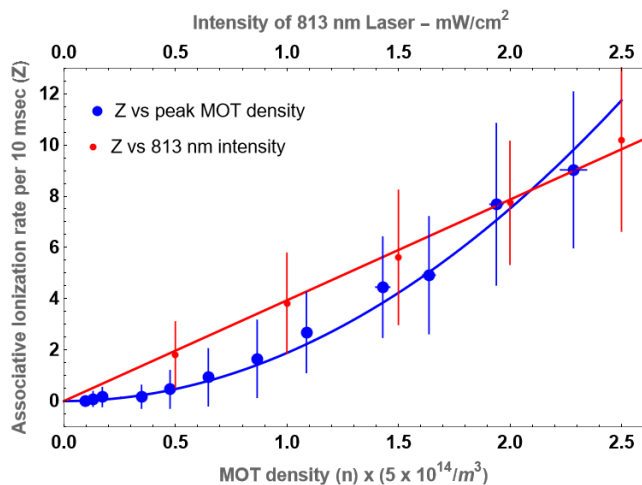


FIG. 11. Variation of the associative ionization rate with the intensity of the 813 nm laser and with the peak MOT density. We note that the data just shows the trend of the variation of the associative ionization rate and not absolute numbers: they can be different in reality depending on the efficiency of detection, and on the overlap between the MOT (with FWHM of  $\approx 1 \text{ mm}$ ) and the 813 nm beam (with diameter of  $\approx 1 \text{ mm}$ ) for a particular measurement set.

- 
- [1] W. W. Smith, O. P. Makarov, and J. Lin, Cold ion-neutral collisions in a hybrid trap, *Journal of Modern Optics* **52**, 2253 (2005).
  - [2] A. T. Grier, M. Cetina, F. Oručević, and V. Vuletić, Observation of cold collisions between trapped ions and trapped atoms, *Physical review letters* **102**, 223201 (2009).
  - [3] C. Zipkes, S. Palzer, C. Sias, and M. Köhl, A trapped single ion inside a bose-einstein condensate, *Nature* **464**, 388 (2010).
  - [4] F. H. Hall, M. Aymar, N. Bouloufa-Maafa, O. Dulieu, and S. Willitsch, Light-assisted ion-neutral reactive processes in the cold regime: Radiative molecule formation versus charge exchange, *Physical review letters* **107**, 243202 (2011).
  - [5] K. Ravi, S. Lee, A. Sharma, G. Werth, and S. Rangwala, Combined ion and atom trap for low-temperature ion-atom physics, *Applied Physics B* **107**, 971 (2012).
  - [6] S. Haze, S. Hata, M. Fujinaga, and T. Mukaiyama, Observation of elastic collisions between lithium atoms and



- calcium ions, *Phys. Rev. A* **87**, 052715 (2013).
- [7] S. Jyothi, T. Ray, N. B. Ram, and S. Rangwala, *Hybrid ion, atom and light trap*, Vol. 189 (IOS Press, 2015).
- [8] H. López, B. Höltkemeier, J. Glässel, P. Weckesser, M. Weidemüller, T. Best, E. Endres, and R. Wester, Sympathetic cooling of oh<sup>-</sup> ions using ultracold rb atoms in a dark spot, in *Ion Traps for Tomorrow's Applications* (IOS Press, 2015) pp. 279–287.
- [9] E. R. Hudson, Sympathetic cooling of molecular ions with ultracold atoms, *EPJ Techniques and Instrumentation* **3**, 1 (2016).
- [10] Z. Meir, T. Sikorsky, R. Ben-shlomi, N. Akerman, M. Pinkas, Y. Dallal, and R. Ozeri, Experimental apparatus for overlapping a ground-state cooled ion with ultracold atoms, *Journal of Modern Optics* **65**, 501 (2018).
- [11] S. Jyothi, K. N. Egodapitiya, B. Bondurant, Z. Jia, E. Pretzsch, P. Chiappina, G. Shu, and K. R. Brown, A hybrid ion-atom trap with integrated high resolution mass spectrometer, *Review of Scientific Instruments* **90** (2019).
- [12] H. Hirzler, T. Feldker, H. Fürst, N. V. Ewald, E. Trimby, R. S. Lous, J. D. Arias Espinoza, M. Mazzanti, J. Joger, and R. Gerritsma, Experimental setup for studying an ultracold mixture of trapped Yb<sup>+</sup>-<sup>6</sup>Li, *Phys. Rev. A* **102**, 033109 (2020).
- [13] J. Schmidt, P. Weckesser, F. Thielemann, T. Schaetz, and L. Karpa, Optical traps for sympathetic cooling of ions with ultracold neutral atoms, *Physical review letters* **124**, 053402 (2020).
- [14] C. Veit, N. Zuber, O. Herrera-Sancho, V. Anasuri, T. Schmid, F. Meinert, R. Löw, and T. Pfau, Pulsed ion microscope to probe quantum gases, *Physical Review X* **11**, 011036 (2021).
- [15] M. Tomza, K. Jachymski, R. Gerritsma, A. Negretti, T. Calarco, Z. Idziaszek, and P. S. Julienne, Cold hybrid ion-atom systems, *Rev. Mod. Phys.* **91**, 035001 (2019).
- [16] K. Ravi, S. Lee, A. Sharma, G. Werth, and S. Rangwala, Cooling and stabilization by collisions in a mixed ion-atom system, *Nature communications* **3**, 1126 (2012).
- [17] S. Dutta and S. Rangwala, Cooling of trapped ions by resonant charge exchange, *Physical Review A* **97**, 041401 (2018).
- [18] S. Jyothi, T. Ray, S. Dutta, A.-R. Allouche, R. Vexiau, O. Dulieu, and S. Rangwala, Photodissociation of trapped rb 2+: Implications for simultaneous trapping of atoms and molecular ions, *Physical review letters* **117**, 213002 (2016).
- [19] T. Sikorsky, Z. Meir, R. Ben-Shlomi, N. Akerman, and R. Ozeri, Spin-controlled atom-ion chemistry, *Nature communications* **9**, 920 (2018).
- [20] T. Stoecklin, P. Halvick, M. A. Gannouni, M. Hochlaf, S. Kotochigova, and E. R. Hudson, Explanation of efficient quenching of molecular ion vibrational motion by ultracold atoms, *Nature Communications* **7**, 11234 (2016).
- [21] A. Mahdian, A. Krüchow, and J. H. Denschlag, Direct observation of swap cooling in atom-ion collisions, *New Journal of Physics* **23**, 065008 (2021).
- [22] M. Pinkas, O. Katz, J. Wengrowicz, N. Akerman, and R. Ozeri, Trap-assisted formation of atom-ion bound states, *Nature Physics* **19**, 1573 (2023).
- [23] P. Weckesser, F. Thielemann, D. Wiater, A. Wojciechowska, L. Karpa, K. Jachymski, M. Tomza, T. Walker, and T. Schaetz, Observation of feshbach resonances between a single ion and ultracold atoms, *Nature* **600**, 429 (2021).
- [24] N. Zuber, V. S. Anasuri, M. Berngruber, Y.-Q. Zou, F. Meinert, R. Löw, and T. Pfau, Observation of a molecular bond between ions and rydberg atoms, *Nature* **605**, 453 (2022).
- [25] S. Lee, K. Ravi, and S. Rangwala, Measurement of collisions between rubidium atoms and optically dark rubidium ions in trapped mixtures, *Physical Review A* **87**, 052701 (2013).
- [26] S. Dutta and S. Rangwala, Measurement of collisions between laser-cooled cesium atoms and trapped cesium ions, *Physical Review A* **102**, 033309 (2020).
- [27] S. Haze, M. Sasakawa, R. Saito, R. Nakai, and T. Mukaiyama, Cooling dynamics of a single trapped ion via elastic collisions with small-mass atoms, *Physical Review Letters* **120**, 043401 (2018).
- [28] J. Joger, H. Fürst, N. Ewald, T. Feldker, M. Tomza, and R. Gerritsma, Observation of collisions between cold li atoms and yb<sup>+</sup> ions, *Physical Review A* **96**, 030703 (2017).
- [29] J. Kwolek, D. Goodman, B. Slayton, R. Blümel, J. Wells, F. Narducci, and W. Smith, Measurement of charge exchange between na and ca<sup>+</sup> in a hybrid trap, *Physical Review A* **99**, 052703 (2019).
- [30] R. Ben-shlomi, R. Vexiau, Z. Meir, T. Sikorsky, N. Akerman, M. Pinkas, O. Dulieu, and R. Ozeri, Direct observation of ultracold atom-ion excitation exchange, *Phys. Rev. A* **102**, 031301 (2020).
- [31] R. Ben-shlomi, M. Pinkas, Z. Meir, T. Sikorsky, O. Katz, N. Akerman, and R. Ozeri, High-energy-resolution measurements of an ultracold-atom-ion collisional cross section, *Physical Review A* **103**, 032805 (2021).
- [32] T. Feldker, H. Fürst, H. Hirzler, N. Ewald, M. Mazzanti, D. Wiater, M. Tomza, and R. Gerritsma, Buffer gas cooling of a trapped ion to the quantum regime, *Nature Physics* **16**, 413 (2020).
- [33] A. Krüchow, A. Mohammadi, A. Härter, J. H. Denschlag, J. Pérez-Ríos, and C. H. Greene, Energy scaling of cold atom-atom-ion three-body recombination, *Physical Review Letters* **116**, 193201 (2016).
- [34] A. Mohammadi, A. Krüchow, A. Mahdian, M. Deiß, J. Pérez-Ríos, H. da Silva Jr, M. Raoult, O. Dulieu, and J. H. Denschlag, Life and death of a cold barb<sup>+</sup> molecule inside an ultracold cloud of rb atoms, *Physical Review Research* **3**, 013196 (2021).
- [35] X. Xing, H. da Silva Jr., R. Vexiau, N. Bouloufa-Maafa, S. Willitsch, and O. Dulieu, Ion-loss events in a hybrid trap of cold rb-ca<sup>+</sup>: Photodissociation, blackbody radiation, and nonradiative charge exchange, *Phys. Rev. A* **106**, 062609 (2022).
- [36] C.-h. Iu, G. D. Stevens, and H. Metcalf, Instrumentation for multistep excitation of lithium atoms to rydberg states, *Applied optics* **34**, 2640 (1995).
- [37] G. D. Stevens, C.-H. Iu, S. Williams, T. Bergeman, and H. Metcalf, Hyperfine splitting of the 3 2 s state of li 7 measured using stark spectroscopy of rydberg states, *Physical Review A* **51**, 2866 (1995).
- [38] J. R. Rubbmark, M. M. Kash, M. G. Littman, and D. Kleppner, Dynamical effects at avoided level crossings: A study of the landau-zener effect using rydberg atoms, *Physical Review A* **23**, 3107 (1981).
- [39] M. G. Littman, M. M. Kash, and D. Kleppner, Field-ionization processes in excited atoms, *Physical Review*

- Letters **41**, 103 (1978).
- [40] A. Drakoudis, M. Söllner, and G. Werth, Instabilities of ion motion in a linear paul trap, *International Journal of Mass Spectrometry* **252**, 61 (2006).
- [41] M. Sinhal and S. Willitsch, Molecular-ion quantum technologies, *Photonic Quantum Technologies: Science and Applications* **1**, 305 (2023).
- [42] F. G. Major, V. N. Gheorghe, and G. Werth, *Charged particle traps: physics and techniques of charged particle field confinement*, Vol. 37 (Springer Science & Business Media, 2005).
- [43] X. Zhao, V. Ryjkov, and H. Schuessler, Parametric excitations of trapped ions in a linear rf ion trap, *Physical Review A* **66**, 063414 (2002).
- [44] B. Collings, W. Stott, and F. Londry, Resonant excitation in a low-pressure linear ion trap, *Journal of the American Society for Mass Spectrometry* **14**, 622 (2003).
- [45] N. Šibalić, J. D. Pritchard, C. S. Adams, and K. J. Weatherill, Arc: An open-source library for calculating properties of alkali rydberg atoms, *Computer Physics Communications* **220**, 319 (2017).
- [46] P. Oxley and P. Collins, Frequency stabilization of multiple lasers and rydberg atom spectroscopy, *Applied Physics B* **101**, 23 (2010).
- [47] M. Aymar and O. Dulieu, Calculation of accurate permanent dipole moments of the lowest  $1,3\Sigma^+$  states of heteronuclear alkali dimers using extended basis sets, *J. Chem. Phys.* **122**, 204302 (2005).
- [48] R. Vexiau, D. Borsalino, M. Lepers, A. Orbán, M. Aymar, O. Dulieu, and N. Bouloufa-Maafa, Dynamic dipole polarizabilities of heteronuclear alkali dimers: optical response, trapping and control of ultracold molecules, *Int. Rev. Phys. Chem.* **36**, 709 (2017).
- [49] O. Dulieu, A. Giusti-Suzor, and F. Masnou-Seeuws, Theoretical treatment of the associative ionization reaction between two laser-excited sodium atoms. direct and indirect processes, *Journal of Physics B: Atomic, Molecular and Optical Physics* **24**, 4391 (1991).
- [50] O. Dulieu, S. Magnier, and F. Masnou-Seeuws, Doubly-excited states for the na 2 molecule: application to the dynamics of the associative ionization reaction, *Zeitschrift für Physik D Atoms, Molecules and Clusters* **32**, 229 (1994).
- [51] O. Dulieu, Application of quantum defect theory to the associative ionisation reaction between two laser-excited sodium atoms, in *Topics in Atomic and Nuclear Collisions* (Springer, 1994) pp. 291–301.
- [52] P. Polak-Dingels, J. Keller, J. Weiner, J.-C. Gauthier, and N. Bras, Observation of laser-induced associative ionization in crossed-beam na+ li collisions, *Physical Review A* **24**, 1107 (1981).
- [53] P. Polak-Dingels, J.-F. Delpech, and J. Weiner, Observation of structure in laser-induced penning and associative ionization in crossed-beam na+ na collisions, *Physical Review Letters* **44**, 1663 (1980).
- [54] X. Urbain, A. Cornet, F. Brouillard, and A. Giusti-Suzor, Dynamics of an elementary bond-forming process: Associative ionization in h (1s)+ h (2s) collisions, *Physical review letters* **66**, 1685 (1991).
- [55] A. v. Hellfeld, J. Caddick, and J. Weiner, Observation of laser-induced penning and associative ionization in li-li collisions, *Physical Review Letters* **40**, 1369 (1978).
- [56] E. Babenko, C. Tapalian, and W. Smith, Associative ionization in laser-excited sodium 3p+ 3d collisions, *Chemical physics letters* **244**, 121 (1995).
- [57] C. Gabbanini, M. Biagini, S. Gozzini, A. Lucchesini, and L. Moi, Associative ionization in collisions between na (3 p 3/2) and cs (6 p 3/2), *Physical Review A* **43**, 2311 (1991).
- [58] M. McGeoch, R. Schlier, and G. Chawla, Associative ionization with cold rydberg lithium atoms, *Physical review letters* **61**, 2088 (1988).
- [59] Y. Ono, I. Koyano, and I. Tanaka, Mass spectrometric detection of cs2+ produced by associative ionization, *The Journal of Chemical Physics* **52**, 5969 (1970).
- [60] J. Blangé, J. Zijlstra, A. Amelink, X. Urbain, H. Rudolph, P. Van der Straten, H. Beijerinck, and H. Heideman, Vibrational state distribution of na 2+ ions created in ultracold collisions, *Physical review letters* **78**, 3089 (1997).
- [61] J. Weiner, *Cold and ultracold collisions in quantum microscopic and mesoscopic systems* (Cambridge University Press, 2003).
- [62] M. Trachy, G. Veshapidze, M. Shah, H. Jang, and B. DePaola, Photoassociation in cold atoms via ladder excitation, *Physical review letters* **99**, 043003 (2007).
- [63] P. Gould, P. Lett, P. Julienne, W. Phillips, H. Thorsheim, and J. Weiner, Observation of associative ionization of ultracold laser-trapped sodium atoms, *Physical review letters* **60**, 788 (1988).
- [64] A. Pandey, R. Vexiau, L. G. Marcassa, O. Dulieu, and N. Bouloufa-Maafa, Ultracold charged atom-dimer collisions: state-selective charge exchange and three-body recombination (2024), arXiv:2407.14824 [physics.atom-ph].
- [65] S. Miyake, C. Gay, and P. Stancil, Rovibrationally resolved photodissociation of heh+, *The Astrophysical Journal* **735**, 21 (2011).
- [66] S. Chu, L. Hollberg, J. E. Bjorkholm, A. Cable, and A. Ashkin, Three-dimensional viscous confinement and cooling of atoms by resonance radiation pressure, *Physical review letters* **55**, 48 (1985).
- [67] E. W. McDaniel, *Collision Phenomena in Ionized Gases* (Wiley, New York, 1964).
- [68] A. Härter and J. Hecker Denschlag, Cold atom-ion experiments in hybrid traps, *Contemporary Physics* **55**, 33 (2014).
- [69] N. Kurz, *Kinematically complete multiphoton ionization studies on optically trapped 6Li and 6Li2 created by single-color photoassociation*, Ph.D. thesis, Ruprecht-Karls-Universität Heidelberg (2021).
- [70] N. Ewald, T. Feldker, H. Hirzler, H. Fürst, and R. Gerritsma, Observation of interactions between trapped ions and ultracold rydberg atoms, *Physical Review Letters* **122**, 253401 (2019).
- [71] T. Dieterle, M. Berngruber, C. Hölzl, R. Löw, K. Jachymski, T. Pfau, and F. Meinert, Inelastic collision dynamics of a single cold ion immersed in a bose-einstein condensate, *Physical Review A* **102**, 041301 (2020).
- [72] M. Deiß, S. Haze, and J. Hecker Denschlag, Long-range atom-ion rydberg molecule: a novel molecular binding mechanism, *Atoms* **9**, 34 (2021).
- [73] P. Kumar and V. Natarajan, Precise measurement of hyperfine structure in the 3s1/2 state of 7li, *Scientific Reports* **7**, 13204 (2017).